JACS
JOURNAL OF THE AMERICAN CHEMICAL SOCIETY
Communication
pubs.acs.org/JACS

Amyloid Fibril Disruption by Ultrasonic Cavitation: Nonequilibrium Molecular Dynamics Simulations

Hisashi Okumura*[,†,‡] and Satoru G. Itoh[†,‡]

[†]Research Center for Computational Science, Institute for Molecular Science, Okazaki, Aichi 444-8585, Japan
[‡]Department of Structural Molecular Science, The Graduate University for Advanced Studies, Okazaki, Aichi 444-8585, Japan

Web-Enhanced Feature *Supporting Information*

ABSTRACT: We describe the disruption of amyloid fibrils of Alzheimer's amyloid-β peptides by ultrasonic cavitation. For this purpose, we performed nonequilibrium all-atom molecular dynamics simulations with sinusoidal pressure and visualized the process with movies. When the pressure is negative, a bubble is formed, usually at hydrophobic residues in the transmembrane region. Most β-strands maintain their secondary structures in the bubble. When the pressure becomes positive, the bubble collapses, and water molecules crash against the hydrophilic residues in the nontransmembrane region to disrupt the amyloid. Shorter amyloids require longer sonication times for disruption because they do not have enough hydrophobic residues to serve as a nucleus to form a bubble. These results agree with experiments in which monodispersed amyloid fibrils were obtained by ultrasonication.

Amyloid fibrils are insoluble aggregates of misfolded fibrous proteins associated with more than 20 human neurodegenerative diseases,[1−3] For example, Alzheimer's disease is caused by amyloid-β (Aβ) peptides, Huntington's disease is related to a polyglutamine, the causative substance of Parkinson's disease is α-synuclein, and dialysis-related amyloidosis results from deposition of β2-microglobulin. To overcome these diseases, it is essential to understand amyloid genesis and disruption. Ultrasonic waves have been widely used to study the extension and disruption of amyloid fibrils. Ultrasonication induces the formation of amyloid fibrils in monomeric solutions of amyloidogenic proteins.[4−6] When ultrasonication is continued, the preformed amyloid fibrils are broken down into shorter fibrils.[5,7] It has been suggested that cavitation may occur and disrupt the amyloid fibrils,[4] but the mechanism of fibril extension and disruption is still unknown.

Here, we focus on how cavitation (the formation of bubbles in liquids) breaks down amyloid fibrils at the atomic level. This conformational change occurs too quickly to be detected by experiments. Because this is a nonlinear nonequilibrium phenomenon including a liquid−gas phase transition, it also cannot be dealt with by analytical theory. Molecular dynamics (MD) simulation is a powerful theoretical tool for understanding atomic-level phenomena. There is, however, no MD simulation for bubble dynamics in a biomolecular system with an amyloid fibril. Nonequilibrium MD simulations in biomolecular systems have been performed usually within a linear response. Nonlinear phenomena with a phase transition have been rarely treated even in nonlinear nonequilibrium simulations. Some MD simulations for bubble formation, growth, and collapse have been conducted for relatively simple liquids such as Lennard-Jones liquid[8,9] and water[9,10] but not in a biomolecular system. There are several MD simulations of Aβ peptide aggregation,[11−13] but there have been no MD simulations of amyloid fibril disruption conducted to date. In this study, we performed such simulations and investigated the mechanism of amyloid disruption by ultrasonic waves. Through these MD simulations, we clarified how bubbles are formed and how they break down the amyloid fibrils.

We first modeled an amyloid fibril with 12 Aβ peptides (residues 17−42) from an experimental conformation (PDB: 2BEG),[14] as shown in Figure 1a. The amyloid fibril of Aβ has two intermolecular β-sheets: one, called β1, is in the nontransmembrane (NTM) region (residues 17−28) and the other, called β2, is in the transmembrane (TM) region (residues 29−42). We then performed an equilibrium MD simulation of the Aβ fibril in explicit water. Starting from the equilibrated conformations, one of which is shown in Figure 1b, we performed nonequilibrium MD simulations with sinusoidal pressure as illustrated in Figure 1c to mimic the ultrasonic wave. Twenty different initial conditions were used for statistical analysis. The Generalized-

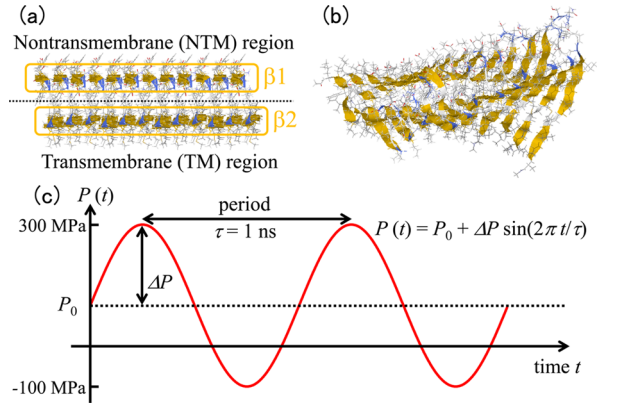

Figure 1. (a) Amyloid fibril conformation modeled from an experimental conformation. (b) One of the initial conformations for the nonequilibrium MD simulations obtained after equilibration. (c) Sinusoidal evolution of the set pressure as a function of time. Conformations in (a) and (b) were created with RasMol.[15]

Received: March 18, 2014
Published: July 2, 2014

   dx.doi.org/10.1021/ja502749f | J. Am. Chem. Soc. 2014, 136, 10549−10552

Ensemble Molecular Biophysics (GEMB) program developed by one of the authors (H.O.)[16] was used to perform the MD simulations. The AMBER parm99SB force field[17] was used for the Aβ peptides, and the TIP3P rigid-body model[18] was used for the water molecules. Temperature was controlled at 298 K with the Nosé–Hoover thermostat.[19] Pressure was controlled with the Andersen barostat.[20] The symplectic[21] quaternion scheme was used for the rigid-body water molecules.[22] See Supporting Information (SI) for the simulation details.

Movie 1 shows a typical MD simulation, and snapshots are shown in Figure 2. Nothing happened to the amyloid when

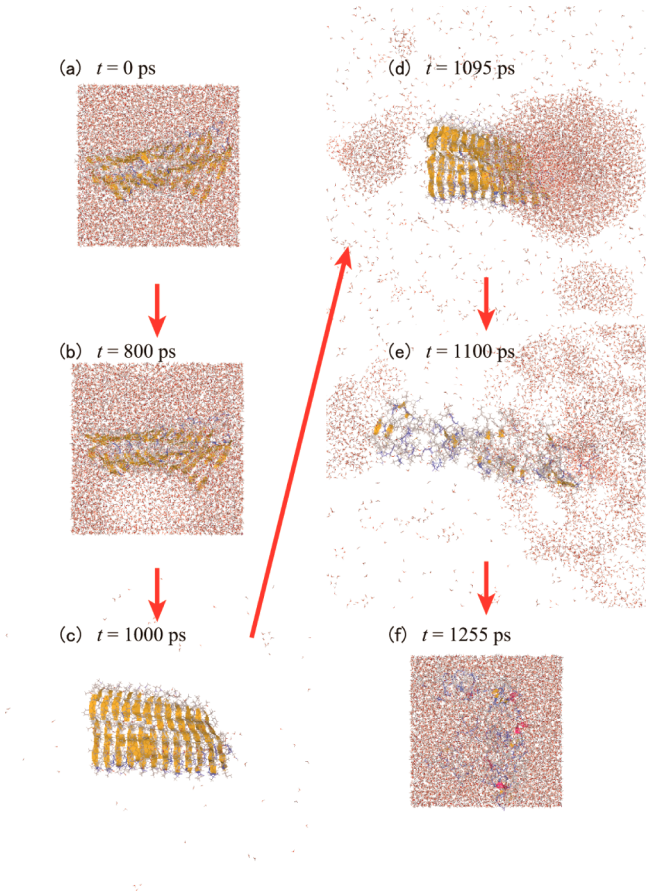

Figure 2. MD simulation of Aβ fibril disruption by cavitation. See Movie 1 and Movie 2.

pressure was positive. When pressure became negative, a bubble was formed at hydrophobic residues in the TM region. The amyloid kept its structure even in the bubble. When the bubble collapsed after pressure became positive again, water molecules crashed against hydrophilic residues in the NTM region, and the amyloid was disrupted. Although a bubble was usually created at hydrophobic residues in the TM region, as shown in Movie 1, we also found that a bubble was formed at hydrophobic residues in the NTM region in one MD simulation. This process is shown in Movie 2.

Detailed analysis of the MD simulation of Movie 1 and Figure 2 is shown in Figure 3. The other MD trajectories are shown in the SI. Figure 3a shows the time series of the number of hydration water molecules per amino acid residue $N_{H_2O}/N_{residue}$. There were more water molecules around the hydrophilic residues in the NTM region than around the hydrophobic residues in the NTM and TM regions before the bubble was

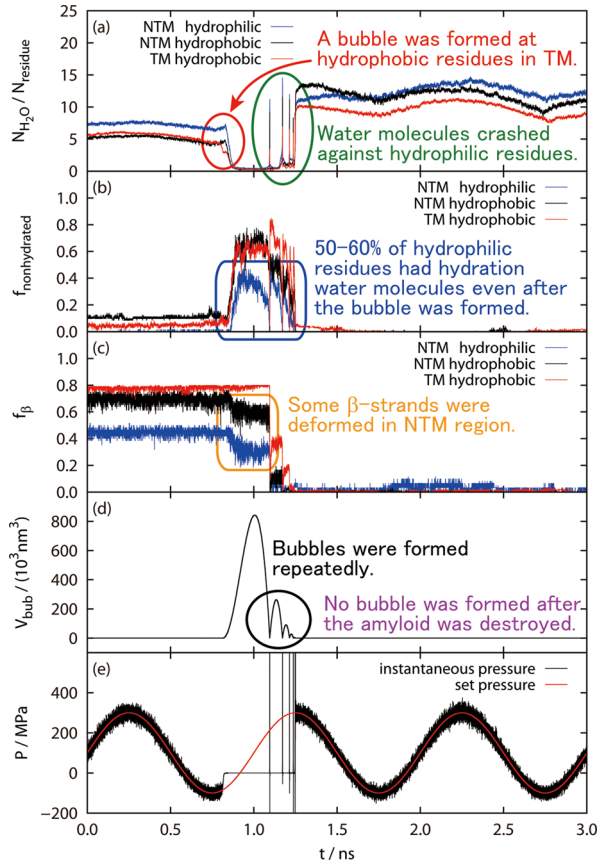

Figure 3. Time series of (a) the number of hydration water molecules per residue, (b) the fraction of nonhydrated residues, (c) the fraction of β-sheet, (d) bubble volume, and (e) pressure. The results in (a–c) were calculated for the hydrophilic and hydrophobic residues in the NTM region and the hydrophobic residues in the TM region. Note that there are no hydrophilic residues in the TM region.

formed. When the bubble was formed, the number of hydration water molecules decreased first around the hydrophobic residues in the TM region. This means that the bubble was formed around the hydrophobic residues in the TM region. The fraction of amino acid residues that had no hydration water molecules $f_{nonhydrated}$ is shown in Figure 3b. Before the bubble was created, most of the residues had at least one hydration water molecule. Once the bubble was formed, the number of residues that had no hydration water molecules increased. The hydrophilic residues in the NTM region had the lowest $f_{nonhydrated}$ (40–50%). Although few water molecules are seen around the amyloid fibril in the movies, 50–60% of the hydrophilic residues in the NTM region retained at least one hydration water molecule.

The fraction of residues that formed β-sheets f_β is shown in Figure 3c. It was determined using the algorithm define secondary structure of proteins (DSSP). Although the hydrophobic residues in the TM region retained the highly formed β-sheet structure, f_β of the hydrophilic and hydrophobic residues in the NTM region decreased after bubble formation. This is because Glu22 and Asp23 in the NTM region deformed the β-sheet structure. Both residues have negative electric charges. The repulsion between them is shielded in water but not in the bubble, which is why the β-sheet structure in the NTM region was deformed in the bubble.

The time series of bubble volume V_{bub} is given in Figure 3d. The bubble was formed, grew, shrank, and collapsed. Once the

dx.doi.org/10.1021/ja502749f | J. Am. Chem. Soc. 2014, 136, 10549–10552

bubble had collapsed, another smaller bubble was formed. Such formation and collapse of the bubble was repeated four or five times in all 20 MD simulations. This phenomenon has also been observed in pure liquids using MD simulations[23] and hydrodynamic calculations.[24] It occurs because the temperature increases locally and instantaneously when the bubble collapses, and water evaporates to form the next bubble. When the bubble collapsed, there were sharp peaks in $N_{H_2O}/N_{residue}$, as seen in Figure 3a. In particular, the hydrophilic residues in the NTM region had the highest peak. This indicates that water molecules crashed against the hydrophilic residues in the NTM region as jet flow, as is well-known in cavitation experiments.[25] The $N_{H_2O}/N_{residue}$ peak of the hydrophobic residues in the NTM region was also high because they are close to the hydrophilic residues. The amyloid fibril was then broken down, as shown in Figure 3c. The time series of pressure is shown in Figure 3e. When there was no bubble, the instantaneous pressure fluctuated around the set pressure. It became almost zero when the bubble was formed and increased sharply when the bubble collapsed.

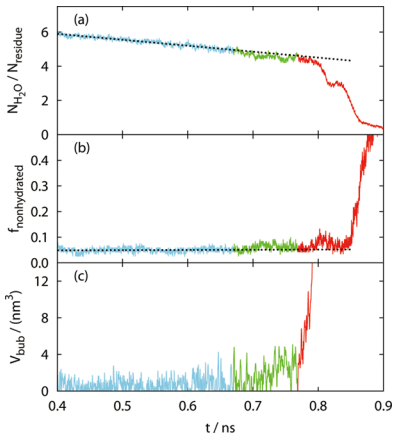

Figure 4. Time series of (a) $N_{H_2O}/N_{residue}$, (b) $f_{nonhydrated}$, and (c) V_{bub} before and after bubble formation. The results for the hydrophobic residues in the TM region are shown in (a) and (b). The fitted lines were obtained by linear fitting of the data, while the set pressure P was relatively low and negative ($P > -75$ MPa, blue lines).

Figure 4 shows the time series of $N_{H_2O}/N_{residue}$, $f_{nonhydrated}$, and V_{bub} before and after bubble formation, which are color-coded into three sections. In the first section (blue), the set pressure P was relatively low and negative ($P > -75$ MPa). The second (green) and third (red) sections are before and after the bubble was formed, respectively. Before the bubble was formed, small bubbles or cavities formed and collapsed several times, as shown in the second section of the V_{bub} time series in Figure 4c. $N_{H_2O}/N_{residue}$ and $f_{nonhydrated}$ for hydrophobic residues in the TM region are lower and higher, respectively, than the fitted lines obtained by linear fitting of the data, while P was low and negative. As these results show, the formation and collapse of cavities is repeated, and the large bubble is finally formed when the cavity size becomes larger than some critical size, as in classical nucleation theory. We note that a bubble can be formed even in the absence of solutes, but it is known that the formation of a bubble is accelerated around hydrophobic molecules.[10] Because the attraction between water and hydrophobic molecules is weaker than that among water molecules, a cavity is easily formed on a hydrophobic surface under negative pressure.

Once the amyloid fibril had been disrupted by the series of bubbles, no bubble was formed again during the 10 ns MD simulation, as shown in Figure 3d, except in one trajectory. This result indicates that if the Aβ peptides exist separately in water, they have little ability to serve as a nucleus to form a bubble. We then performed MD simulations with shorter Aβ fibrils, a hexamer and a trimer. Figure 5 shows how many times pressure had been negative before bubbles were formed in the 20 MD simulations from different initial conditions. In the dodecamer system, a bubble was formed at the first negative pressure in 14 of the 20 MD simulations. A bubble was formed at the second and third negative pressures in 4 and 2 MD simulations, respectively. The hexamer was disrupted at the first negative pressure in 8 MD simulations. At the second and third negative pressures, bubble formation was observed in 4 MD simulations. A bubble was formed at the fourth negative pressure in 2 MD simulations. At the sixth and eighth negative pressures, a bubble was formed in 1 MD simulation. In all cases, the amyloid fibrils were disrupted when the bubbles collapsed. On the other hand, a bubble was formed, and the amyloid was disrupted only in 1 MD simulation in the trimer system. These results clearly show that it is more difficult for a shorter amyloid to be a nucleus for bubble formation. The TM region mainly consists of hydrophobic residues, which can be the nucleus for bubble formation. In the case of short amyloid fibrils, the hydrophobic residues do not gather enough to be a nucleus and more time is required for bubble formation.

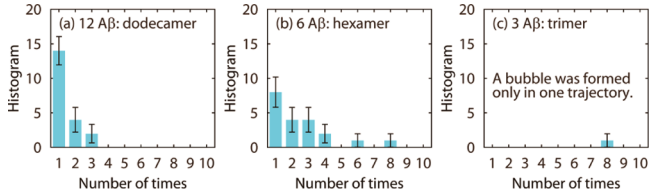

Figure 5. Histograms showing how many times pressure had been negative before bubbles were formed in the (a) dodecamer, (b) hexamer, and (c) trimer systems. Error bars represent standard errors calculated by the bootstrap method.[26] The number of bootstrap cycles was 1×10^7.

Chatani et al. found that amyloid fibrils were broken down into shorter fibrils by ultrasonication, and the lengths of the amyloid fibrils were almost the same.[5] This can be explained by our MD simulations. If the amyloid fibril is longer than some critical length, the hydrophobic residues can serve as a nucleus for bubble formation, and the bubble breaks down the fibrils. On the other hand, if the amyloid fibril is not long enough, the hydrophobic residues cannot serve as a nucleus, and the amyloid fibrils are not disrupted. This is why ultrasonication results in amyloid fibrils of nearly the same length.

The highest pressure P_{max}, lowest pressure P_{min}, reference pressure P_0, and frequency f in our simulations are different from those in experiments to allow us to observe bubble formation and collapse in a reasonable simulation time. Pressure (~0.1 MPa) and frequency (~20 kHz) in most experiments[5] are lower than those in our simulations. Bubble formation depends on the magnitude and period of negative pressure. A bubble is easily formed under high negative pressure. The period of negative pressure can be changed by P_{max}, P_{min}, P_0, and f. As the period of negative pressure increases, a bubble can be formed more easily.

dx.doi.org/10.1021/ja502749f | J. Am. Chem. Soc. 2014, 136, 10549−10552

P_{min} in the present MD simulations makes bubble formation easier, while the present negative pressure period makes it more difficult than under the usual experimental conditions. Additional MD simulations under different pressure conditions yield the same trends as shown in the SI.

In conclusion, we performed nonequilibrium MD simulations of an Aβ fibril in explicit water with sinusoidal pressure to understand the molecular mechanism of Aβ fibril disruption by ultrasonic cavitation. When the pressure was positive, no significant change was observed in the β-sheet structures. After the pressure became negative, a bubble was created, usually around the TM region, which mainly consists of hydrophobic residues. The fibril retained most of the β-sheet structures even in the bubble. When the pressure became positive again, the bubble shrank and collapsed, and water molecules crashed against the hydrophilic residues in the NTM region. The amyloid fibril was then disrupted. We also investigated the length dependence of bubble formation using the dodecamer, hexamer, and trimer of the Aβ peptides. Disruption of shorter amyloids required more time of negative pressure because the assembly of hydrophobic residues in the TM region acts as a nucleus for bubble formation. If the fibril is too short, it does not have enough hydrophobic residues to create a bubble. This result is consistent with experiments[5] in which monodispersed amyloid fibrils were obtained by ultrasonication. These simulation results have provided an understanding of amyloid disruption at the atomic level, although the size and time scale of the present MD system are smaller than those of the experiments.

There are some ways to make the present MD simulations more realistic. For example, when dissolved gases exist in water, these gases may form a bubble first, while water vapor formed a bubble in the present simulations. In addition, there is a view that ultrasonication-dependent fragmentation is caused by shearing forces produced by the repeated growth and collapse of bubbles.[25] To realize this situation, multiple bubbles should be formed. It is also known that ultrasonication accelerates the formation of fibrils from monomers.[5] One possible scenario is that proteins aggregate on the surface of bubbles formed by ultrasonication because amyloid fibril formation is triggered on the liquid−gas interface.[27] To answer these questions, larger and longer MD simulations will be necessary. These simulations would yield insight about the mechanism of amyloidogenesis and provide useful information to overcome the amyloid diseases.

■ ASSOCIATED CONTENT

Ⓢ Supporting Information

Simulation details and additional data. This material is available free of charge via the Internet at http://pubs.acs.org.

Ⓦ Web-Enhanced Features

Movies of typical MD simulations are available.

■ AUTHOR INFORMATION

Corresponding Author

hokumura@ims.ac.jp

Notes

The authors declare no competing financial interest.

■ ACKNOWLEDGMENTS

This work was supported by JSPS KAKENHI (23740325 and 26102550) and the Okazaki Orion project. We used supercomputers at the Research Center for Computational Science, Okazaki Research Facilities, National Institutes of Natural Sciences.

■ REFERENCES

(1) Sipe, J. D.; Cohen, A. S. *J. Struct. Biol.* **2000**, *130*, 88.
(2) Chiti, F.; Dobson, C. M. *Annu. Rev. Biochem.* **2006**, *75*, 333.
(3) Chiti, F.; Dobson, C. M. *Nat. Chem. Biol.* **2009**, *5*, 15.
(4) Ohhashi, Y.; Kihara, M.; Naiki, H.; Goto, Y. *J. Biol. Chem.* **2005**, *280*, 32843.
(5) Chatani, E.; Lee, Y. H.; Yagi, H.; Yoshimura, Y.; Naiki, H.; Goto, Y. *Proc. Natl. Acad. Sci. U.S.A.* **2009**, *106*, 11119.
(6) Stathopulos, P. B.; Scholz, G. A.; Hwang, Y.; Rumfeldt, J. A. O.; Lepock, J. R.; Meiering, E. M. *Protein Sci.* **2004**, *13*, 3017.
(7) Carulla, N.; Caddy, G. L.; Hall, D. R.; Zurdo, J.; Gairí, M.; Feliz, M.; Giralt, E.; Robinson, C. V.; Dobson, C. M. *Nature* **2005**, *436*, 554.
(8) (a) Kinjo, T.; Ohguchi, K.; Yasuoka, K.; Matsumoto, M. *Comput. Mater. Sci.* **1999**, *14*, 138. (b) Xiao, C.; Heyes, D. M.; Powles, J. G. *Mol. Phys.* **2002**, *100*, 3451. (c) Okumura, H.; Ito, N. *Phys. Rev. E* **2003**, *67*, 045301(R). (d) Watanabe, H.; Suzuki, M.; Ito, N. *Phys. Rev. E* **2010**, *82*, 051604.
(9) Takahashi, H.; Morita, A. *Chem. Phys. Lett.* **2013**, *573*, 35.
(10) Koishi, T.; Yoo, S.; Yasuoka, K.; Zeng, X. C.; Narumi, T.; Susukita, R.; Kawai, A.; Furusawa, H.; Suenaga, A.; Okimoto, N.; Futatsugi, N.; Ebisuzaki, T. *Phys. Rev. Lett.* **2004**, *93*, 185701.
(11) Itoh, S. G.; Okamoto, Y. *J. Phys. Chem. B* **2008**, *112*, 2767.
(12) O'Brien, E. P.; Okamoto, Y.; Straub, J. E.; Brooks, B. R.; Thirumalai, D. *J. Phys. Chem. B* **2009**, *113*, 14421.
(13) Nguyen, P. H.; Li, M. S.; Stock, G.; Straub, J. E.; Thirumalai, D. *Proc. Natl. Acad. Sci. U.S.A.* **2007**, *104*, 111.
(14) Luhrs, T.; Ritter, C.; Adrian, M.; Riek-Loher, D.; Bohrmann, B.; Dobeli, H.; Schubert, D.; Riek, R. *Proc. Natl. Acad. Sci. U.S.A.* **2005**, *102*, 17342.
(15) Sayle, R. A.; Milner-White, E. J. *Trends Biochem. Sci.* **1995**, *20*, 374.
(16) (a) Okumura, H.; Okamoto, Y. *J. Phys. Chem. B* **2008**, *112*, 12038. (b) Okumura, H. *Proteins* **2012**, *80*, 2397. (c) Okumura, H.; Itoh, S. G. *Phys. Chem. Chem. Phys.* **2013**, *15*, 13852.
(17) Hornak, V.; Abel, R.; Okur, A.; Strockbine, B.; Roitberg, A.; Simmerling, C. *Proteins* **2006**, *65*, 712.
(18) Jorgensen, W. L.; Chandrasekhar, J.; Madura, J. D.; Impey, R. W.; Klein, M. L. *J. Chem. Phys.* **1983**, *79*, 926.
(19) (a) Nosé, S. *Mol. Phys.* **1984**, *52*, 255. (b) Nosé, S. *J. Chem. Phys.* **1984**, *81*, 511. (c) Hoover, W. G. *Phys. Rev. A* **1985**, *31*, 1695.
(20) Andersen, H. C. *J. Chem. Phys.* **1980**, *72*, 2384.
(21) Yoshida, H. *Phys. Lett. A* **1990**, *150*, 262.
(22) (a) Miller, T. F.; Eleftheriou, M.; Pattnaik, P.; Ndirango, A.; Newns, D.; Martyna, G. J. *J. Chem. Phys.* **2002**, *116*, 8649. (b) Okumura, H.; Itoh, S. G.; Okamoto, Y. *J. Chem. Phys.* **2007**, *126*, 084103.
(23) Matsumoto, M. *J. Therm. Sci. Technol. (Tokyo, Jpn.)* **2008**, *3*, 309.
(24) Lugli, F.; Zerbetto, F. *Phys. Chem. Chem. Phys.* **2007**, *9*, 2447.
(25) Phull, S. S.; Mason, T. J. The Uses of Ultrasound for Biological Decontamination. In *Advances in Sonochemistry*; Mason, T. J., Tiehm, A., Eds.; Elsevier: Amsterdam, 2001; Vol. 6, pp 1−23.
(26) Efron, B. *Ann. Stat.* **1979**, *7*, 1.
(27) Hoernke, M.; Falenski, J. A.; Schwieger, C.; Koksch, B.; Brezenski, G. *Langmuir* **2011**, *27*, 14218.